CrossMark

RESEARCH PAPER

Synthesis and characterization of nanostructured iron compounds prepared from the decomposition of iron pentacarbonyl dispersed into carbon materials with varying porosities

Miguel A. Schettino Jr. · Alfredo G. Cunha · Evaristo Nunes · Edson C. Passamani · Jair C. C. Freitas · Francisco G. Emmerich · Milton K. Morigaki

Abstract This work describes the production and characterization of carbon-iron nanocomposites obtained from the decomposition of iron pentacarbonyl ($Fe(CO)_5$) mixed with different carbon materials: a high surface area activated carbon (AC), powdered graphite (G), milled graphite (MG), and carbon black (CB). The nanocomposites were prepared either under argon or in ambient atmosphere, with a fixed ratio of $Fe(CO)_5$ (4.0 mL) to carbon precursor (2.0 g). The images of scanning electron microscopy and the analysis of textural properties indicated the presence of nanostructured Fe compounds homogeneously dispersed into the different classes of pores of the carbon matrices. The elemental Fe content was always larger for samples prepared in ambient atmosphere, reaching values in the range of 20–32 wt%. On the other hand, samples prepared under argon showed reduced Fe content, with values in the range 5–10 wt% for samples prepared from precursors with low surface area (G, MG, and CB) and a much higher value ($\sim$19 wt%) for samples prepared from the precursor of high surface area (AC). Mössbauer spectroscopy and X-ray diffractometry showed that the nanoparticles were mostly composed of iron oxides in the case of the samples prepared in oxygen-rich ambient atmosphere and also for the AC-derived nanocomposite prepared under argon, which is consistent with the large oxygen content of this precursor. For the other precursors, with reduced or no oxygen content, metallic iron and iron carbides were found to be the dominant phases in samples prepared under oxygen-free atmosphere. The samples prepared in ambient atmosphere and the AC-derived sample prepared under argon exhibited superparamagnetic behavior at room temperature, as revealed by temperature-dependent magnetization curves and Mössbauer spectroscopy.

Keywords Iron oxides · Porous carbon · Iron pentacarbonyl · Mössbauer spectroscopy · X-ray diffraction · α-Fe · ZFC/FC · Nanocomposites

M. A. Schettino Jr. (✉) · A. G. Cunha · E. Nunes · E. C. Passamani · J. C. C. Freitas · F. G. Emmerich
Departamento de Física, Universidade Federal do Espírito Santo, 29075-910 Vitória, ES, Brazil
e-mail: miguel.ufes@gmail.com

M. K. Morigaki
Departamento de Química, Universidade Federal do Espírito Santo, 29075-910 Vitória, ES, Brazil

Introduction

Nanocomposites are composite materials where at least one of their components has one of the dimensions in the size range less than 100 nm (Camargo et al. 2009). The methods used to synthesize nanocomposites exert great influence on their physical and chemical characteristics, including chemical composition, stoichiometry, crystal structure, microstructure, electric

and magnetic properties, among others (Gleiter 1992). The search for low-cost and easily reproducible methods of synthesis of nanocomposites is a subject of high current interest, especially for materials with large perspectives for technological applications, such as the carbon-iron nanocomposites. The potential applications of these nanocomposites are several, including: industrial optimization (Ramsden 2009), deployment of new biomedical techniques for treatments and prevention of disease (Davis 2002), cost reduction in civil construction (Steyn 2009), improvement in the quality and production of agricultural products (Galembeck et al. 2007), preparation of ferrofluid solutions (Sun and Nava 2002), adsorbing contaminants in water (Gupta et al. 2011), adsorption and oxidation by Fenton processes (Oliveira et al. 2010) and others.

One of the major concerns in nanocomposites synthesis is the production of an uniform material (morphology, size and distribution of particle size) with reproducible physical, chemical and magnetic properties. This aim is a difficult task due to the small particle size of some components (Willard et al. 2004). Among the various synthesis methods, the wet preparation is the most economically viable. In this method, the precursors are either in liquid state or in solution. The properties of the nanoproducts obtained by wet preparation methods (such as impregnation, precipitation, co-precipitation, etc.) depend strongly on the conditions used during the synthesis, including the temperature, the pH of the reaction medium, the possible use of catalysts, the possible application of electric fields, ultrasound, electromagnetic radiation and others (Ragheb et al. 2013; Klabunde and Richards 2009; Koch 2006). There are also many recent examples of nanoparticles of metal oxides produced by wet chemical routes starting from metal complexes (Hosny 2014; Hosny et al. 2015, 2016b; Snovski et al. 2014; Schettino Jr et al. 2010; Moussa et al. 2013).

There are various possible combinations of materials for the production of nanocomposites, including zeolite-encapsulated iron oxide nanoparticles (Luo et al. 2015; Lai et al. 2015) and silica nanoparticles in mixed matrix membranes (Jullok et al. 2016). However, because of the versatile characteristics of carbon materials as well as the physical and chemical properties of iron compounds, one of the most promising types of nanocomposites involves the combination iron-carbon. A wide diversity of carbon materials, such as pitches, carbon fibers, activated carbons, carbon blacks, graphite, and carbon nanotubes have been mentioned as suitable nanoparticle supports (Sano et al. 2003). Within this group, activated carbon offer some advantages, since they have weak interaction with dispersed nanoparticles, besides presenting high specific surface area and wide distribution of pore sizes (Minchev et al. 2005). However, activated carbons have structural and physical properties largely dependent on the chemical features of the carbon precursor and on the specific conditions employed during the synthesis (Camargo et al. 2009; Rudge et al. 2000; Alexandrescu et al. 2010).

Iron-containing nanoparticles dispersed in activated carbons are among the most frequently investigated nanocomposites. In wet preparation methods, as the iron source must be in solution, the compounds iron(III) nitrate nonahydrate, iron(II) chloride, iron(III) chloride, ferrocene, iron carbonyls, etc., are used in many of the reported works (Kharisov et al. 2012; Huber 2005; Lu et al. 2007; Mohapatra and Anand 2010; Wu et al. 2009). Among the iron oxides, magnetite (Fe_3O_4) and maghemite (γ-Fe_2O_3) embedded in a carbon matrix are by far the most studied ones, due to the large interest in view of technological applications. Another interesting iron-carbon compound is cementite (Fe_3C), because it shows very good chemical stability and high saturation magnetization (Schnepp et al. 2010). However, it is relatively difficult to obtain pure Fe_3C phase. High temperatures and special conditions are required for the reduction of Fe-oxides, which leads to the formation of a mixture of Fe and Fe_3C or even only metallic α-Fe (Cheng et al. 2011). Despite elemental iron presenting a much higher saturation magnetization than its oxides, the Fe particles are easily oxidized, leading to a significant reduction in their saturation magnetization. This problem, however, can be avoided by protecting the Fe particles with a shell, which may be composed of a carbon-based material(Snovski et al. 2012).

Our previous works (Schettino Jr et al. 2010, 2012) show that it is possible to produce nanoparticles of iron oxides supported on an activated carbon matrix, by the decomposition of $Fe(CO)_5$. We show that different results can be obtained, depending on the details of the synthesis conditions; likewise, the subsequent thermal treatments (atmosphere N_2) are extremely important to consolidate the phase and the size of desired

particles. Particularly, it is possible to obtain nanoparticles of hematite α-Fe_2O_3 diluted in activated carbon matrix or to synthesize crystalline hematite, depending on the atmosphere and the heat treatment temperature. Similar results were obtained in the studies by Hosny et al. (2016a, b) for hematite synthesized from poly o-aminophenol.

In this work, we investigated the role played by the carbon matrix on the nature and properties of iron-based nanoparticles produced by the decomposition of the $Fe(CO)_5$. This substance was chosen as the source of iron, due to the interesting features of having iron in the zero-valence state (Fe^0) and presenting low activation energy for breaking the Fe-CO bonds. It is a liquid with high vapor pressure at room temperature, being thus easily decomposed to form iron compounds dispersed into the carbon matrix (Jäger et al. 2006; Schettino Jr et al. 2010, 2012; Huber 2005). Four different carbon materials with varying porosities were used as support for the iron-based nanoparticles: a high-surface area activated carbon (AC), powdered graphite (G), milled graphite (MG), and carbon black (CB). Different types of iron compounds were produced in nanostructured forms, including iron oxides, carbides and metallic iron, depending on the physical and chemical characteristics (notably on the oxygen content and surface area) of each carbon precursor.

Experimental methods

One iron compound precursor and four carbon material precursors were utilized. $Fe(CO)_5$ (Aldrich) was used as received. AC is a commercial charcoal activated carbon powder (Merck, product number 102186). Powdered graphite (G) was obtained by grinding a high-purity graphite rod (Alfa Aesar, 99.9995 %, product number 14739) in an agate mortar. MG was obtained by milling G for 4h in a high energy mill. The milling was carried out in a vibrating mill table, where container and cylinder are made tempered steal with a hardness of 65 HRc and volumes of 176 and 89 cm^3, respectively. About 10 g of G was placed in the container under ambient atmosphere and temperature. CB was produced as a solid deposit resulting from the plasma pyrolysis of vehicular natural gas (Cunha et al. 2012). All carbon precursors were ground and sieved to 70 mesh before impregnation with $Fe(CO)_5$.

All samples were prepared using the same ratio of $Fe(CO)_5$ (4.0 mL) to carbon precursor (2.0 g). Two different synthesis methods were employed: (i) In the first method, liquid $Fe(CO)_5$ was directly added to the carbon powder, at room temperature and ambient atmosphere, in an open Petri dish. The mixture was kept in a fume hood for about seven days, until the complete drying of the material. The samples prepared according to this method were labeled as AMB samples. (ii) In the second method, each carbon precursor was placed in a Schlenk flask coupled to a Friedrichs condenser (with continuous water flow) and purged with argon flow at atmospheric pressure for 3 h. Next, liquid $Fe(CO)_5$ was added using a syringe. The system was kept in a thermal bath at 115 °C for 12 h and then it was evacuated until the complete drying of the mixture. The samples prepared according to this method were labeled as ARG samples.

The chemical composition of the samples was determined by elemental analysis (C, H, N, O contents), using a Leco CHNS-932 coupled to a VTF-900 furnace (for O analysis). Thermogravimetry (TG) curves were recorded in a Shimadzu TGA-50H instrument, under O_2 or N_2 flow (20 mL/min) using a heating-rate of 5 °C/min up to the final temperature of 1000 °C. The Fe content was estimated from the ash content of the samples, which was determined from the residual weight observed after complete combustion of the materials under oxidizing atmosphere up to 1000 °C in the TG apparatus. This calculation was carried out considering that the ashes were entirely composed of hematite (Fe_2O_3), as identified by X-ray diffraction (XRD) and Mössbauer spectroscopy (Schettino Jr et al. 2010, 2012). The correctness of such assumption was verified by checking that the sum of the values of all determined atomic contents was close to 100 % (with error <2 wt%). XRD patterns were recorded at room temperature, using a Shimadzu XRD-6000 diffractometer, with Cu-Kα radiation (λ = 1.5418 Å) and 2θ values ranging from 10 to 90 °C in steps of 0.05 °C. Mössbauer spectra (MS) were recorded in a conventional transmission geometry, both at room temperature (RT) and at 20 K, using a[57]Co:Rh radioactive source at RT. All isomer shift values were corrected with respect to the bulk α-Fe value obtained at RT. The morphology of the samples was investigated by scanning electron microscopy (SEM), using a Shimadzu SSX-550 instrument. Energy dispersive X-ray spectroscopy (EDX) analyses

were recorded using a SEDX-500 instrument coupled to the scanning electron microscope. Textural analysis was performed from the N_2 adsorption/desorption isotherms recorded at 77 K, using a Quantachrome Autosorb instrument, with specific surface area (SSA) values determined using the BET method (Brunauer et al. 1938). The magnetic properties of the samples were investigated using an evercool-I physical properties measurement system (PPMS), from Quantum Design. Both zero field cooled (ZFC) and field cooled (FC) magnetization curves were recorded with magnetic field intensity of $H = 500$ Oe and the magnetization M was normalized to sample weight. Alternate current (a.c.) magnetic susceptibility measurements as a function of temperature were also performed, using a small a.c. magnetic field (10 Oe), a frequency of 1.0 kHz and, optionally, a superimposed constant magnetic field (500 Oe).

Results and discussion

Table 1 gives the elemental analysis data and SSA of the as-synthesized nanocomposites and the carbon precursors. The elemental Fe contents in the synthesized materials were always higher for samples prepared in ambient atmosphere, with the highest values occurring for AC and CB (both ~ 32 wt%). It is interesting to observe the good correlation between the Fe and O contents in all synthesized samples, which suggests the presence of iron oxides as one of the major formed phases in the samples. In the case of ARG samples, the increase in the O contents of the

nanocomposites was caused by the decomposition of $Fe(CO)_5$. Comparing the carbon precursors among themselves, it is observed that the O contents increase proportionally to the SSA values, in the order AC > MG > CB > G. The sample G, with the lowest O content and the smallest SSA value, was the precursor giving rise to the nanocomposites with the most reduced Fe contents. The effect of milling was clearly noted, leading to an increase in SSA and O content of the MG precursor as compared to G and in the Fe content of the derived nanocomposites.

Figure 1 shows the TG curves recorded under N_2 flow for AMB (a) and ARG (b) samples. All AMB samples showed an intense and sharp weight loss in the temperature range 700–750 °C. This feature was observed before in other iron-carbon nanocomposites, being associated with the reduction of nanostructured iron oxides to form mainly metallic iron nanoparticles (Schettino Jr et al. 2010, 2012). The magnitude of the weight loss was directly related to the O content of each material, which can be observed by comparing the TG curves of AMB and ARG samples. The weight-loss corresponding to the iron oxides reduction was present in the TG curve recorded for the sample AC-ARG (which is rich in oxygen, due to the large O content of the precursor AC). The sample MG-ARG (the second in O content among the ARG samples) showed a much slighter loss at a higher temperature, whereas the other samples presented no corresponding weight loss.

Figure 2 shows the XRD patterns recorded for the synthesized nanocomposites, with the angular positions corresponding to graphite and to some iron

Table 1 Elemental analysis data (in wt%) and specific surface area values for all samples

| Sample	C (%)	H (%)	N (%)	O (%)	Fe (%)	SSA (m^2/g)
AC	79.8 (1)	2.6 (1)	0.50 (1)	14.6 (6)	–	1333
AC-AMB	40.7 (1)	1.70 (8)	0.20 (1)	27.0 (1)	31.5 (1)	756
AC-ARG	62.3 (6)	2.0 (1)	0.20 (5)	18.4 (4)	19.4 (3)	826
CB	98.5 (5)	0.2 (2)	1.1 (1)	0.28 (7)	–	54
CB-AMB	51 (1)	0.5 (1)	0.62 (5)	19.2 (1)	32.0 (1)	30
CB-ARG	83.3 (3)	0.03 (1)	0.80 (3)	1.20 (6)	10.2 (1)	50
MG	99.0 (2)	0.03 (3)	0.40 (1)	1.24 (6)	–	110
MG-AMB	58.8 (7)	0.89 (2)	0.30 (6)	16.0 (1)	24.7 (1)	80
MG-ARG	91.0 (4)	0.16 (9)	0.40 (8)	3.0 (2)	7.8 (1)	95
G	100.3 (2)	0.02 (1)	0.10 (6)	0.04 (1)	–	8
G-AMB	63.7 (2)	0.48 (44)	0.45 (1)	13.2 (3)	20.2 (2)	11
G-ARG	92.5 (7)	0.04 (1)	0.20 (3)	0.37 (3)	5.3 (1)	7
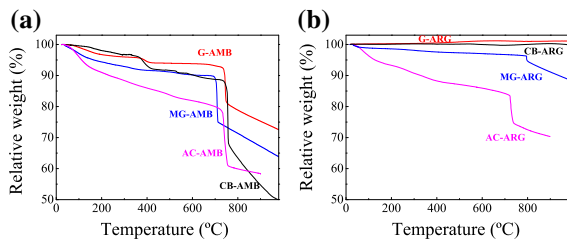
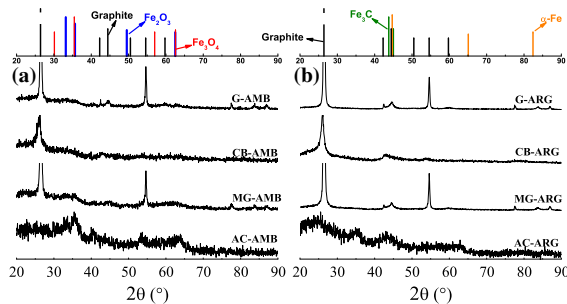**Fig. 1** TG curves recorded under N_2 flow for **a** AMB and **b** ARG samples

Fig. 2 XRD patterns recorded for **a** AMB and **b** ARG samples. The angular positions corresponding to graphite and to some iron compounds are shown at the *top*

compounds likely to have been formed during the synthesis shown at the top. The XRD patterns did not show the presence of diffraction peaks associated with any crystalline phases of iron compounds. Apart from the Bragg peaks associated with graphite (in G- and MG-derived samples) or turbostratic carbon (in AC- and CB-derived samples), only broad bands identified with nanosized iron compounds were observed in these XRD patterns. Diffraction bands in the angular range corresponding to iron oxides were clearly observed in AC-AMB and AC-ARG samples and, with minor intensity, in the other AMB samples (Schettino Jr et al. 2010, 2012). This is consistent with the previously discussed large O and Fe contents of these samples as compared to the other ones. The average crystallite sizes of these nanostructured iron oxides, estimated from the inverse linewidth of the corresponding broad bands, were found to be around 5 nm.

The SEM images and the corresponding EDX spectra recorded for the nanocomposites (shown in Fig. 3) indicated that all iron compounds were homogeneously dispersed throughout the carbon matrices within the observation scale length (~ 5 µm). The images clearly showed the distinct

morphologies of the as-prepared nanocomposites, which are related to the differences in the carbon precursors used in each case. The typical morphologies expected for a charcoal (Marsh and Reinoso 2006) and for a carbon black (Donnet 1993) were observed in the SEM images of the AC-derived and CB-derived (Fig. 3) samples, respectively, with no evidence for the segregation of Fe-containing particles. The comparison of the SEM images recorded for the MG-derived and G-derived materials (Fig. 3) also revealed the changes caused by milling, with the presence of small rounded, less-faceted particles in the nanocomposite prepared from the milled graphite (Knieke et al. 2010; Antisari et al. 2006). The EDX spectra, shown in the insets of Fig. 3, exhibited the Fe characteristic peaks with intensities in the order AC > CB > MG > G, in agreement with the elemental analysis data of ARG samples given in Table 1.

The RT Mössbauer spectra of all AMB samples (Fig. 4a) were fitted using only a quadrupole splitting distribution component. The broad nature of these spectra is attributed to the chemical and structural disorder around the ^{57}Fe nuclei in the nanostructured iron compounds (Schettino Jr et al. 2010). The hyperfine parameters were roughly the same for all AMB samples, with approximate values of 0.34 and 0.7 mm/s for the isomer shift and mean quadrupole splitting, respectively. These values are in accordance with what would be expected for Fe^{3+} oxides (Greenwood and Gibb 1971). These results suggest that similar compounds (identified as nanostructured iron oxides) were formed in all samples synthesized in
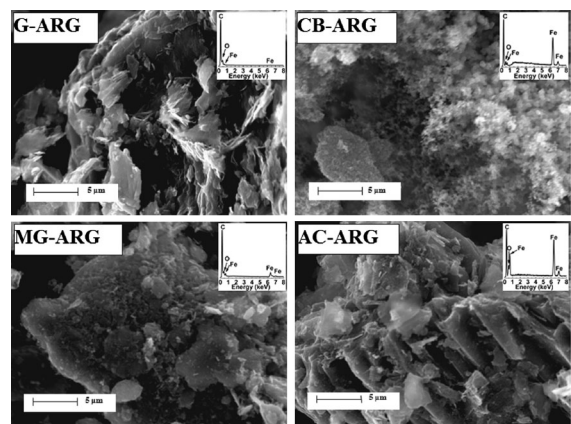

Fig. 3 SEM images of the samples G-ARG, CB-ARG, MG-ARG, and AC-ARG
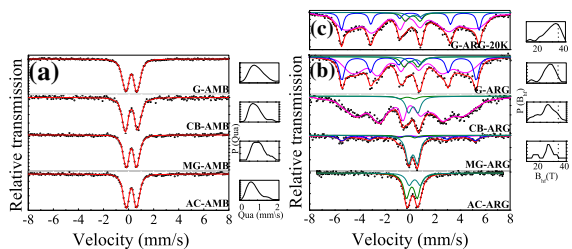
Fig. 4 Mössbauer spectra recorded at room temperature for the **a** AMB and **b** ARG samples, in **c** it is shown the spectrum recorded at 20 K for the G-ARG sample

oxygen-rich ambient atmosphere, irrespective of the different Fe amounts present in each material.

On the other hand, the RT Mössbauer spectra of the ARG samples (Fig. 4b) were somewhat more complex. In the case of AC-ARG sample, two broad doublets were used for fitting the spectrum, with isomer shifts of 0.27 and 0.55 mm/s and quadrupole splittings of 0.86 mm/s for both components. These values and the relative area of the subspectra (in the ratio of ca. 2:1) point to the presence of Fe^{3+} and Fe^{2+} components associated with magnetite (Schettino Jr et al. 2012; Karr 1978; Orolínová and Mockovčiaková 2009). This is consistent with the reduced O contents of the samples synthesized under argon atmosphere. In the case of the other ARG samples, similar doublets were also used for fitting the spectra, which suggests that nanostructured magnetite is one of the phases present in these samples as well. Besides these components, broad distributions of magnetic hyperfine field (B_{hf}) were required for fitting the Mössbauer spectra of samples G-ARG, MG-ARG, and CB-ARG, with mean B_{hf} values around 26 T. The range of B_{hf} values found in these distributions is consistent with the presence of iron carbides and metallic Fe nanoparticles, in agreement with previous reports of materials prepared from the decomposition of $Fe(CO)_5$ (Minchev et al. 2005; Snovski et al. 2014). The Mössbauer spectra of samples G-ARG and MG-ARG also showed the presence of a well-defined sextet (very intense in the case of sample G-ARG) with isomer shift $\cong 0.0$ mm/s and $B_{hf} \cong 33$ T, indicating clearly the formation of α-Fe nanoparticles (Pérez-Cabero et al. 2006; Greenwood and Gibb 1971). It is interesting to note that these nanoparticles are stable in air in ambient conditions. The Mössbauer spectrum of sample G-ARG recorded at 20 K, Fig. 4c, was also fitted using the same components present in the RT

spectrum, only with a shift in the mean value of the B_{hf} distribution to ~34 T, indicating the predominance of α-Fe phase in this sample.

Figure 5 shows the temperature-dependent magnetization curves, M(T), recorded for the AMB and ARG samples, following the ZFC and FC protocols. The shapes of the ZFC curves obtained for samples G-AMB, MG-AMB, CB-AMB were very similar, with the occurrence of a magnetization maximum at a temperature close to 50 K, identified as the blocking temperature (T_B) (Guimarães 1998) of the magnetic moments of the nanoparticles that are in the
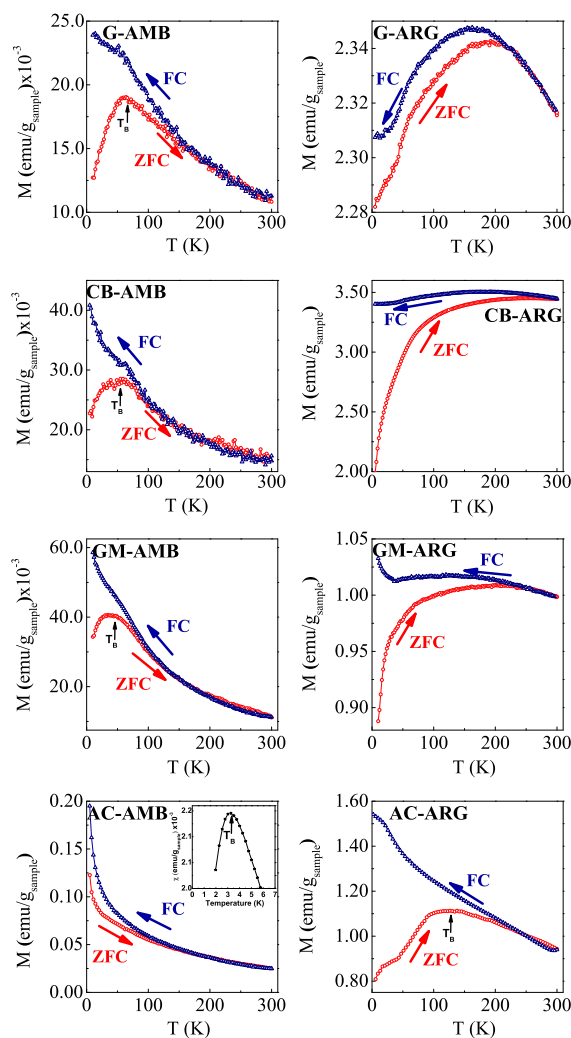

Fig. 5 ZFC and FC magnetization curves recorded for the AMB and ARG samples. The *inset* in the *left bottom* part shows the real part of the a.c. magnetic susceptibility curve recorded under a constant magnetic field of 500 Oe

superparamagnetic regime at RT. In all these cases, the ZFC and FC curves were found to deviate from each other in a broad range of temperatures below RT and above T_B. This suggests the occurrence of a wide particle size distribution for the synthesized Fe-based nanoparticles, with particles of different sizes (and thus with distinct individual blocking temperatures) being progressively blocked as the temperature is reduced (Allia et al. 2013; Schettino Jr et al. 2012).

The ZFC and FC M(T) curves recorded for the sample AC-AMB exhibited similar features, with the important exception that no maximum in the ZFC curve was observed down to 5 K. However, a maximum in the temperature-dependent alternate current magnetic susceptibility curve, χ_{AC} (T), shown in the inset in the left bottom part of Fig. 5, was observed at ca. 3.5 K with the application of a constant magnetic field of 500 Oe. This evidence suggests that the nanoparticles present in this nanocomposite are very small in size, in agreement with the above discussed XRD and Mössbauer spectroscopy data, remaining in the unblocked regime at quite low temperatures. The continuous increase of the magnetization with decreasing temperature in the FC M(T) curve recorded for the AC-AMB sample was an indication of weak interparticle interactions in this nanocomposite, in spite of its large Fe content (31.5 wt%, see Table 1) (Prené et al. 1993; Papusoi Jr 1999; Vargas et al. 2005). This is consistent with a scenario where the fine nanoparticles are homogeneously dispersed throughout the porous matrix of the AC support (Schettino Jr et al. 2012). On the other hand, slight changes in the slope of the FC M(T) curves in the low temperature range (below T_B) were observed for the CB-AMB, MG-AMB, and G-AMB samples, which might be an indication of an increase in the strength of interparticle interactions in these cases (Vargas et al. 2005).

In contrast, the profiles of the M(T) curves recorded for most ARG samples (Fig. 5) were remarkably distinct from the ones observed for AMB samples. In the case of AC-ARG sample, the ZFC and FC curves were still consistent with the expected behavior of a material that is superparamagnetic at room temperature. However, the maximum in the ZFC curve (at ca. 125 K) was broad and ill-defined, whereas the thermal irreversibility in the magnetization was observed to start at temperatures far above T_B, which suggests the occurrence of a broad particle size distribution in this

material (Yu et al. 1995). The M(T) curves recorded for the other ARG samples exhibited a more complex behavior, with the occurrence of thermal irreversibility in a broad range of temperatures. Also, both the ZFC and the FC curves recorded for these samples exhibited maxima at different temperatures and a minimum was observed in the FC curves at low temperatures. These features suggest the occurrence of strong interparticle interactions and of the formation of a cluster glass (or superspin glass) state at low temperatures (Bedanta and Kleemann 2009; Zysler et al. 2001).

These differences in the magnetic behavior between AMB and ARG samples are easy to understand considering the details of their composition, revealed by Mössbauer spectroscopy. While all AMB samples and also the AC-ARG sample are basically composed of nanostructured Fe^{3+} oxides, a mixture of nanoparticles composed of metallic iron, iron carbides, and magnetite was identified by Mössbauer spectroscopy in the CB-ARG, MG-ARG, and G-ARG samples. Considering the occurrence of ferromagnetic or ferrimagnetic phases at RT in these materials (as revealed by the presence of sextets and B_{hf} distributions in the Mössbauer spectra), the M(T) values of ARG samples were relatively high in comparison with the values observed for AMB samples, even though the Fe contents of ARG samples were always lower than the corresponding contents of AMB samples (see Table 1). With the reduction in the temperature, the occurrence of intraparticle and interparticle magnetic interactions in these complex mixtures caused the complex behavior observed in the FC and ZFC curves shown in Fig. 5.

Conclusions

Nanostructured iron compounds were prepared inside different carbon matrices, giving rise to carbon-iron nanocomposites. The nature of these iron compounds was largely influenced by the conditions used in the synthesis (especially regarding the presence of oxygen in the synthesis atmosphere) and the chemical/physical characteristics of the carbon precursors (such as the oxygen content and the internal surface area). For samples prepared under ambient atmosphere, nanostructured Fe^{3+} oxides (with average crystallite size around 5 nm) were the dominant phases, with Fe contents in the range 20–32 wt%. On the other hand,

materials prepared under argon atmosphere showed the presence of nanostructured iron carbides and metallic iron, mixed with iron oxides in different amounts for the various carbon precursors. In the case of the sample prepared from an oxygen-free precursor (graphite) and under argon atmosphere, the dominant phase was composed of α-Fe nanoparticles, which showed good stability in ambient conditions. Samples prepared at ambient conditions have shown superparamagnetic-like behavior at room temperature, but their blocking temperatures are ca. 50 K for all samples. Since the carbon matrices have a broad distribution of porous, it was also observed this feature in Fe nanoparticles formed during our synthesis.

References

Alexandrescu R, Morjan I, Tomescu A, Simion CE, Scarisoreanu M, Birjega R, Fleaca C, Gavrila L, Soare I, Dumitrache F et al (2010) Direct production of a novel iron-based nanocomposite from the laser pyrolysis of Fe(CO)₅/MMA mixtures: structural and sensing properties. J Nanomater 2010:1

Allia P, Barrera G, Bonelli B, Freyria FS, Tiberto P (2013) Magnetic properties of pure and eu-doped hematite nanoparticles. J Nanoparticle Res 15(12):1–12

Antisari MV, Montone A, Jovic N, Piscopiello E, Alvani C, Pilloni L (2006) Low energy pure shear milling: a method for the preparation of graphite nano-sheets. Scripta Mater 55(11):1047–1050

Bedanta S, Kleemann W (2009) Supermagnetism. J Phys D Appl Phys 42(1):013001

Brunauer S, Emmett PH, Teller E (1938) Adsorption of gases in multimolecular layers. J Am Chem Soc 60(2):309–319

Camargo PHC, Satyanarayana KG, Wypych F (2009) Nanocomposites: synthesis, structure, properties and new application opportunities. Mater Res 12(1):1–39

Cheng X, Wu B, Yang Y, Li Y (2011) Synthesis of iron nanoparticles in water-in-oil microemulsions for liquid-phase fischer-tropsch synthesis in polyethylene glycol. Catal Commun 12(6):431–435

Cunha AG, Freitas JCC, Cipriano DF, Emmerich FG (2012) Solid-state NMR study of carbon blacks obtained by plasma pyrolysis of natural gas extended abstract. In CARBON 2012—The annual world conference on carbon, Krakow, Poland, ID 813

Davis ME (2002) Ordered porous materials for emerging applications. Nature 417:813–818

Donnet JB (1993) Carbon black: science and technology. CRC Press, Boca Raton

Galembeck F, Santos ÁCM, Schumacher HC, Rippel MM, Rosseto R (2007) Chemical industry: recent developments, problems and opportunities. Quim Nova 30(6):1413–1419

Gleiter H (1992) Materials with ultrafine microstructures: retrospectives and perspectives. Nanostruct Mater 1(1):1–19

Greenwood NN, Gibb TC (1971) Mössbauer spectroscopy. Chapman and Hall Ltda, London

Guimarães AP (1998) Magnetism and magnetic resonance in solids. Wiley, New York

Gupta V, Gupta B, Rastogi A, Agarwal S, Nayak A (2011) Pesticides removal from waste water by activated carbon prepared from waste rubber tire. Water Res 45(13):4047–4055

Hosny NM (2014) Single crystalline Co₃O₄: synthesis and optical properties. Mater Chem Phys 144(3):247–251

Hosny NM, Al-Hussaini AS, Nowesser N, Zoromba MS (2015) Polyanthranilic acid. J Therm Anal Calorimet, 1–7

Hosny NM, Nowesser N, Al-Hussaini A, Zoromba MS (2016a) Doped copolymer of polyanthranilic acid and o-aminophenol (AA-co-OAP): synthesis, spectral characterization and the use of the doped copolymer as precursor of α-Fe₂O₃ nanoparticles. J Mol Struct 1106:479–484

Hosny NM, Nowesser N, Al Hussaini A, Zoromba S (2016b) Solid state synthesis of hematite nanoparticles from doped poly o-aminophenol (POAP). J Inorg Organomet Polym Mater 26(1):41–47

Huber DL (2005) Synthesis, properties, and applications of iron nanoparticles. Small 1(5):482–501

Jäger C, Mutschke H, Huisken F, Alexandrescu R, Morjan I, Dumitrache F, Barjega R, Soare I, David B, Schneeweiss O (2006) Iron-carbon nanoparticles prepared by CO₂ laser pyrolysis of toluene and iron pentacarbonyl. Appl Phys A 85(1):53–62

Jullok N, Van Hooghten R, Luis P, Volodin A, Van Haesendonck C, Vermant J, Van der Bruggen B (2016) Effect of silica nanoparticles in mixed matrix membranes for pervaporation dehydration of acetic acid aqueous solution: Plant-inspired dewatering systems. J Clean Prod 112:4879–4889

Karr C (1978) Analytical methods for coal and coal products, vol 2. Academic Press, San Francisco

Kharisov BI, Dias HR, Kharissova OV, Jiménez-Pérez VM, Perez BO, Flores BM (2012) Iron-containing nanomaterials: synthesis, properties, and environmental applications. RSC Advan 2(25):9325–9358

Klabunde KJ, Richards RM (2009) Nanoscale materials in chemistry. Wiley, Chichester

Knieke C, Berger A, Voigt M, Taylor RNK, Röhrl J, Peukert W (2010) Scalable production of graphene sheets by mechanical delamination. Carbon 48(11):3196–3204

Koch CC (2006) Nanostructured materials: processing, properties and applications. William Andrew, New York

Lai Y, Rutigliano MN, Veser G (2015) Controlled embedding of metal oxide nanoparticles in ZSM-5 zeolites through preencapsulation and timed release. Langmuir 31(38):10562–10572

Lu A-H, Salabas EE, Schüth F (2007) Magnetic nanoparticles: synthesis, protection, functionalization, and application. Angew Chem Int Ed 46(8):1222–1244

Luo L, Dai C, Zhang A, Wang J, Liu M, Song C, Guo X (2015) Facile synthesis of zeolite-encapsulated iron oxide nanoparticles as superior catalysts for phenol oxidation. RSC Adv 5(37):29509–29512

Marsh H, Reinoso FR (2006) Activated carbon. Elsevier, Amsterdam

Minchev C, Huwe H, Tsoncheva T, Paneva D, Dimitrov M, Mitov I, Fröba M (2005) Iron oxide modified mesoporous carbons: physicochemical and catalytic study. Microporous Mesoporous Mater 81(1):333–341

Mohapatra M, Anand S (2010) Synthesis and applications of nano-structured iron oxides/hydroxides—a review. Int J Eng Sci Technol 2(8):127–146

Moussa S, Atkinson G, El-Shall MS (2013) Laser-assisted synthesis of magnetic Fe/Fe_2O_3 core: carbon-shell nanoparticles in organic solvents. J Nanoparticle Res 15(3):1–10

Oliveira DQL, Oliveira LCA, Murad E, Fabris JD, Silva AC, de Menezes LM (2010) Niobian iron oxides as heterogeneous fenton catalysts for environmental remediation. Hyperfine Interact 195(13):27–34

Orolínová Z, Mockovčiaková A (2009) Structural study of bentonite/iron oxide composites. Mater Chem Phys 114(2):956–961

Papusoi C Jr (1999) The particle interaction effects in the field-cooled and zero-field-cooled magnetization processes. J Magn Magn Mater 195(3):708–732

Pérez-Cabero M, Taboada JB, Guerrero-Ruiz A, Overweg AR, Rodríguez-Ramos I (2006) The role of alpha-iron and cementite phases in the growing mechanism of carbon nanotubes: a [57]Fe Mössbauer spectroscopy study. Phys Chem Chem Phys 8(10):1230–1235

Prené P, Tronc E, Jolivet J-P, Livage J, Cherkaoui R, Nogues M, Dormann J-L, Fiorani D (1993) Magnetic properties of isolated γ-Fe_2O_3 particles. Magn IEEE Trans 29(6):2658–2660

Ragheb RR, Kim D, Bandyopadhyay A, Chahboune H, Bulutoglu B, Ezaldein H, Criscione JM, Fahmy TM (2013) Induced clustered nanoconfinement of superparamagnetic iron oxide in biodegradable nanoparticles enhances transverse relaxivity for targeted theranostics. Magn Reson Med 70(6):1748–1760

Ramsden J (2009) Applied nanotechnology. William Andrew, Norwich

Rudge SR, Kurtz TL, Vessely CR, Catterall LG, Williamson DL (2000) Preparation, characterization, and performance of magnetic iron-carbon composite microparticles for chemotherapy. Biomaterials 21(14):1411–1420

Sano N, Akazawa H, Kikuchi T, Kanki T (2003) Separated synthesis of iron-included carbon nanocapsules and nanotubes by pyrolysis of ferrocene in pure hydrogen. Carbon 41(11):2159–2162

Schettino MA Jr, Freitas JCC, Morigaki MK, Nunes E, Cunha AG, Passamani EC, Emmerich FG (2010) High-temperature xrd study of thermally induced structural and chemical changes in iron oxide nanoparticles embedded in porous carbons. J Nanoparticle Res 12(8):3097–3103

Schettino MA Jr, Gonçalves GR, Morigaki MK, Nunes E, Cunha AG, Passamani EC, Emmerich FG, Nascente PAP, Freitas JCC (2012) Synthesis, characterization and study of thermal behavior of nanostructured iron oxides embedded in porous carbon prepared from the decomposition of iron pentacarbonyl. In Martinez AI (ed) Iron oxides: structure, properties and applications, Nova Publishers, New York, pp 19–51

Schnepp Z, Wimbush SC, Antonietti M, Giordano C (2010) Synthesis of highly magnetic iron carbide nanoparticles via a biopolymer route. Chem Mater 22(18):5340–5344

Snovski R, Grinblat J, Margel S (2012) Novel magnetic fe onion-like fullerene micrometer-sized particles of narrow size distribution. J Magn Magn Mater 324(1):90–94

Snovski R, Grinblat J, Sougrati MT, Jumas JC, Margel S (2014) Synthesis and characterization of iron, iron oxide and iron carbide nanostructures. J Magn Magn Mater 349:35–44

Steyn WJ (2009) Potential applications of nanotechnology in pavement engineering. J Transp Eng 135(10):764–772

Sun XC, Nava N (2002) Microstructure and magnetic properties of Fe(C) and Fe(O) nanoparticles. Nano Lett 2(7):765–769

Vargas JM, Nunes WC, Socolovsky LM, Knobel M, Zanchet D (2005) Effect of dipolar interaction observed in iron-based nanoparticles. Phys Rev B 72(18):184428

Willard MA, Kurihara LK, Carpenter EE, Calvin S, Harris VG (2004) Chemically prepared magnetic nanoparticles. Int Mater Rev 49(3–4):125–170

Wu W, He Q, Jiang C et al. (2009) Magnetic iron oxide nanoparticles: synthesis and surface functionalization strategies. ChemInform 40(24):i

Yu RH, Zhang XX, Tejada J, Knobel M, Tiberto P, Allia P (1995) Magnetic properties and giant magnetoresistance in melt-spun Co–Cu alloys. J Appl Phys 78(1):392–397

Zysler RD, Fiorani D, Testa AM (2001) Investigation of magnetic properties of interacting Fe_2O_3 nanoparticles. J Magn Magn Mater 224(1):5–11